




Mediation of Cartilage Matrix Degeneration and Fibrillation by Decorin in Post-traumatic Osteoarthritis

Qing Li,¹ Biao Han,¹ Chao Wang,¹ Wei Tong,² Yulong Wei,² Wei-Ju Tseng,² Li-Hsin Han,¹ X. Sherry Liu,² Motomi Enomoto-Iwamoto,³ Robert L. Mauck,⁴ Ling Qin,² Renato V. Iozzo,⁵ David E. Birk,⁶ and Lin Han¹ 

Objective. To elucidate the role of decorin, a small leucine-rich proteoglycan, in the degradation of cartilage matrix during the progression of post-traumatic osteoarthritis (OA).

Methods. Three-month-old decorin-null ($Dcn^{-/-}$) and inducible decorin-knockout (Dcn^{iKO}) mice were subjected to surgical destabilization of the medial meniscus (DMM) to induce post-traumatic OA. The OA phenotype that resulted was evaluated by assessing joint morphology and sulfated glycosaminoglycan (sGAG) staining via histological analysis ($n = 6$ mice per group), surface collagen fibril nanostructure via scanning electron microscopy ($n = 4$ mice per group), tissue modulus via atomic force microscopy–nanoindentation ($n = 5$ or more mice per group) and subchondral bone structure via micro-computed tomography ($n = 5$ mice per group). Femoral head cartilage explants from wild-type and $Dcn^{-/-}$ mice were stimulated with the inflammatory cytokine interleukin-1 β (IL-1 β) in vitro ($n = 6$ mice per group). The resulting chondrocyte response to IL-1 β and release of sGAGs were quantified.

Results. In both $Dcn^{-/-}$ and Dcn^{iKO} mice, the absence of decorin resulted in accelerated sGAG loss and formation of highly aligned collagen fibrils on the cartilage surface relative to the control ($P < 0.05$). Also, $Dcn^{-/-}$ mice developed more salient osteophytes, illustrating more severe OA. In cartilage explants treated with IL-1 β , loss of decorin did not alter the expression of either anabolic or catabolic genes. However, a greater proportion of sGAGs was released to the media from $Dcn^{-/-}$ mouse explants, in both live and devitalized conditions ($P < 0.05$).

Conclusion. In post-traumatic OA, decorin delays the loss of fragmented aggrecan and fibrillation of cartilage surface, and thus, plays a protective role in ameliorating cartilage degeneration.

INTRODUCTION

Post-traumatic osteoarthritis (OA) is the most prevalent form of arthritis in young adults, and often results in long-term detrimental influence on quality of life (1). One hallmark of post-traumatic OA is the irreversible degradation of articular cartilage following traumatic injuries and/or aberrant joint loading, leading to joint dysfunction, pain, and limited locomotion (2). In post-traumatic OA, elevated chondrocyte catabolism results in aggravated proteolysis of the cartilage extracellular matrix (ECM) (3). Aggrecan, the major proteoglycan, is one of the first ECM constituents to undergo fragmentation due to enzymatic cleavage by aggrecanases and matrix metalloproteinases (MMPs). This leads to the disassembly of the aggrecan–hyaluronan (HA) supramolecular

network and the loss of aggrecan from the ECM (4). In turn, the loss of aggrecan impairs cartilage biomechanical functions (5), disrupts chondrocyte mechanotransduction (6), and accelerates the damage of collagen fibrils (7) and formation of fibrocartilage (8), and so contributes to the vicious loop of irreversible cartilage breakdown. Inhibition of aggrecan depletion from degenerative tissue has the potential to delay cartilage degradation, attenuate OA progression, and prolong joint use.

Decorin, a small leucine-rich proteoglycan (SLRP), could play such a role in regulating cartilage degradation in OA (9). Decorin is a class I SLRP characterized by an ~36-kD leucine-rich protein core harboring one chondroitin sulfate or dermatan sulfate glycosaminoglycan chain at its N-terminus (10). One canonical structural function of decorin is to regulate collagen fibril diameter and inter-

Supported by the NIH (grant P30-AR-069619 to the Penn Center for Musculoskeletal Disorders). Dr. Lin Han's work was supported by the NIH (grants AR-066824 and AR-074490) and the NSF (grant CMMI-1662544).

¹Qing Li, PhD, Biao Han, MS, Chao Wang, MS, Li-Hsin Han, PhD, Lin Han, PhD: Drexel University, Philadelphia, Pennsylvania; ²Wei Tong, PhD, Yulong Wei, PhD, Wei-Ju Tseng, MS, MSE, X. Sherry Liu, PhD, Ling Qin, PhD: Perelman School of Medicine, University of Pennsylvania, Philadelphia; ³Motomi Enomoto-Iwamoto, DDS, PhD: University of Maryland, Baltimore; ⁴Robert L. Mauck, PhD: Perelman School of Medicine, University of Pennsylvania and

Corporal Michael J. Crescenz VAMC, Philadelphia, Pennsylvania; ⁵Renato V. Iozzo, MD, PhD: Sidney Kimmel Medical College, Thomas Jefferson University, Philadelphia, Pennsylvania; ⁶David E. Birk, PhD: Morsani School of Medicine, University of South Florida, Tampa.

No potential conflicts of interest relevant to this article were reported.

Address correspondence to Lin Han, PhD, 3141 Chestnut Street, Bossone 718, Philadelphia, PA 19104. E-mail: lh535@drexel.edu.

Submitted for publication January 13, 2020; accepted in revised form March 5, 2020.

fibrillar spacing during fibril assembly in tension-bearing tissues such as tendon, cornea, and skin (11). In cartilage, decorin is actively expressed from the newborn period to adulthood (12), and is one of the most abundant small proteoglycans in the ECM, with a molar concentration (~15 nmoles/ml) similar to that of aggrecan (~20 nmoles/ml) (13). In early human OA, decorin is significantly up-regulated (14,15). Despite this up-regulation, decorin is not released into the synovial fluid at higher levels (16), suggesting that decorin may participate in stabilizing cartilage matrix. It is postulated that this up-regulation may be a compensatory response by chondrocytes to ameliorate cartilage damage (17). This hypothesis is supported by our recent study showing that decorin increases the retention of aggrecan in healthy cartilage ECM (9). However, one recent study showed that decorin-null ($Dcn^{-/-}$) mice develop higher resistance to forced exercise-induced OA, which was attributed to enhanced transforming growth factor β (TGF β) signaling in the absence of decorin, indicating a detrimental role of decorin (18). Given these findings, the role of decorin in OA remains inconclusive.

The objective of this study was to elucidate the role of decorin in cartilage degradation and post-traumatic OA progression in vivo. Mild-to-moderate post-traumatic OA was induced in young adult mice via surgical destabilization of the medial meniscus (DMM) (19). Given the crucial role of decorin in cartilage development (9), we first investigated whether the absence of decorin increased susceptibility to OA in $Dcn^{-/-}$ mice (20). Next, to separate decorin activity in OA from that in normal joint growth, we tested the recently established inducible decorin-knockout (Dcn^{flox}) mouse model (21). We allowed for normal joint growth in these mice, and then induced the knockout of decorin expression at the time of surgical DMM. Thus, the resulting phenotype represents the impact of decorin loss during OA progression, with developmental defects being minimized. In these models, we assessed cartilage damage and sulfated glycosaminoglycan (sGAG) loss, cartilage surface fibrillation and tissue modulus changes, as well as alterations in subchondral bone structure. Furthermore, we tested whether decorin alters chondrocyte catabolism, or the retention of fragmented aggrecan in the matrix, or both, using cartilage explants exposed to inflammatory stimuli. Taken together, our findings pointed to a crucial protective role of decorin in increasing aggrecan retention and inhibiting cartilage surface fibrillation in post-traumatic OA.

MATERIALS AND METHODS

Animal models. $Dcn^{-/-}$ mice (20) and Dcn^{flox} mice ($Dcn^{flox/flox}$ /Rosa26Cre^{ER}) (21) in the C57BL/6 strain were generated as previously described, and were housed in the Calhoun animal facility at Drexel University. To induce the homozygous knockout of the *Dcn* gene in 3-month-old mice, tamoxifen was injected intraperitoneally on 3 consecutive days beginning 1 week prior to surgical DMM at a dose of 3 mg/40 gm body weight in the form of

20 mg/ml suspended in sesame oil (catalog no. S3547; Sigma) with 1% volume/volume benzyl alcohol (catalog no. 305197; Sigma). Quantitative polymerase chain reaction (qPCR) was performed on day 5 to confirm that tamoxifen-induced gene excision reduced the expression of *Dcn* to the baseline level (Supplementary Figure 1, available on the *Arthritis & Rheumatology* web site at <http://onlinelibrary.wiley.com/doi/10.1002/art.41254/abstract>). For $Dcn^{-/-}$ mice, age-matched wild-type (WT) littermates from the breeding of decorin heterozygous ($Dcn^{+/+}$) mice were used as controls. For Dcn^{flox} mice, 2 control groups were used, including Dcn^{flox} mice injected with vehicle (the same amount of sesame oil and benzyl alcohol but without tamoxifen), and WT mice injected with tamoxifen at the same dose and frequency. All mice used in this study were genotyped according to standard procedures (20,21). Animal experiments were approved by the Institutional Animal Care and Use Committee at Drexel University.

Surgical DMM was performed on the right hind knees of 3-month-old male mice for all genotypes, according to an established procedure (19), with Sham surgery performed on the contralateral left knees. Briefly, after anesthesia, the joint capsule was opened and the medial meniscotibial ligament was cut to destabilize the medial meniscus. The Sham surgery was performed by opening the joint capsule in the same manner to expose the ligament, but without further damage. $Dcn^{-/-}$ and WT mice were euthanized 2 or 8 weeks after surgery, and Dcn^{flox} mice and their controls were euthanized 8 weeks after surgery, for further analyses.

Histological analysis and immunofluorescence imaging. Whole murine hind knee joints ($n = 6$ per group) were harvested and fixed in 4% paraformaldehyde, first used for micro-computed tomography (micro-CT) analysis, and then decalcified in 10% EDTA for 4 weeks before being embedded in paraffin for histological analysis. Serial 6- μ m-thick sagittal sections were prepared, and 2 sections out of every consecutive 6 sections of the medial side of the murine knees subjected to Sham operation or DMM were stained with Safranin O–Fast Green. For each joint, ~15 sections were obtained and scored in a blinded manner by 2 observers (QL and CW) using a modified Mankin scale (22). Uncalcified cartilage thickness ($t_{uncalcified}$) and total cartilage thickness (t_{total}) were determined by averaging 6 thickness values evenly distributed across the entire cartilage, according to an established procedure (23). For immunofluorescence imaging of decorin, additional paraffin sections were treated with 0.1% pepsin (catalog no. P7000; Sigma) for antigen retrieval, and blocked with 5% bovine serum albumin (BSA) in phosphate buffered saline (PBS) for 1 hour at room temperature. Sections were first incubated with primary antibody (LF-114; a gift from Dr. Larry W. Fisher, National Institute of Dental and Craniofacial Research, Bethesda, MD) (1:100 dilution) overnight at 4°C, and then with secondary antibody (Alexa Fluor 594; ThermoFisher) (1:500) for 2 hours at room temperature. The sections were washed with PBS, counterstained, mounted with DAPI (Fluoromount-G) (catalog

no. 0100-20; SouthernBiotech), and imaged with a Zeiss Axio Observer microscope (Carl Zeiss).

Additional immunofluorescence imaging was performed on healthy and OA human cartilage specimens obtained from de-identified donors who had undergone total arthroplasty ($n = 3$). Similar to murine specimens, serial paraffin sections were treated with 0.1% pepsin, blocked with 5% BSA in PBS, and incubated with primary antibody (20 $\mu\text{g}/\text{ml}$) (AF-143; R&D Systems) and then secondary antibody (Alexa Fluor 594; ThermoFisher). The specificity of decorin antibodies was confirmed by the staining of isotype controls (1:100) (for mouse specimens, AB37415 [Abcam]; for human specimens, AB-108-C [Novus Biologicals]) (Supplementary Figure 2, available on the *Arthritis & Rheumatology* web site at <http://online.library.wiley.com/doi/10.1002/art.41254/abstract>).

Atomic force microscopy (AFM)-based nanoindentation. Atomic force microscopy (AFM)-based nanoindentation was applied to freshly dissected femoral condyle cartilage ($n = 5$ or more specimens per group), according to an established procedure (23). The indentation tests were performed using borosilicate microspherical colloidal tips ($R \sim 5 \mu\text{m}$; nominal $k \sim 8.9 \text{ N/m}$; HQ:NSC35/tipless/Cr-Au; cantilever A; NanoAndMore) and a Dimension Icon AFM (Bruker Nano) at a rate of $10 \mu\text{m}/\text{second}$ up to $\sim 1 \mu\text{N}$ maximum load in PBS with protease inhibitors (Pierce 88266; ThermoFisher). For each joint, at least 10–15 locations were tested on the load-bearing region of the medial condyle to account for spatial heterogeneity. The effective indentation modulus (E_{ind}) was calculated by fitting each force-indentation depth loading curve with the Hertz model.

Scanning electron microscopy. Scanning electron microscopy was used to quantify the fibril nanostructure on condyle cartilage surfaces, according to an established procedure (24). Immediately after the AFM tests, joints were treated with 0.1% trypsin (catalog no. T7409; Sigma) and 20 units/ml hyaluronidase (catalog no. H3506; Sigma) at 37°C for 24 hours each to remove proteoglycans, fixed with Karnovsky's fixative at room temperature for 3 hours, sequentially dehydrated in graded water-ethanol and ethanol-hexamethyldisilazane mixtures, and air dried overnight ($n = 4$ samples per group). Samples were then coated with $\sim 6\text{-nm}$ -thick platinum and imaged using a Supra 50VP scanning electron microscope (Carl Zeiss) (Supplementary Figure 3, available on the *Arthritis & Rheumatology* web site at <http://onlinelibrary.wiley.com/doi/10.1002/art.41254/abstract>). Collagen fibril alignment angles, θ , were measured using ImageJ, and fitted with von Mises probability density function to calculate the von Mises concentration parameter, κ , a quantitative measure of the degree of fibril alignment (25).

Micro-CT scanning. Micro-CT scanning was performed to assess concurrent changes in subchondral bone 8 weeks after DMM. For mice used for histological analysis, prior to demineralization, knee joints ($n = 5$ per group) were scanned

ex vivo using MicroCT 35 (Scanco Medical) at $6 \mu\text{m}$ isotropic voxel size and smoothed by a Gaussian filter ($\sigma = 1.2$, support = 2.0). Each region of interest (ROI) for subchondral bone plate, subchondral trabecular bone (STB), and medial meniscal ossicles was contoured at a threshold corresponding to 30% of the maximum image gray scale. The subchondral bone plate of the tibia plateau on the medial side central loading region was contoured to calculate the subchondral bone plate thickness (SBP.Th), according to an established procedure (26). STB was contoured on the entire load-bearing ROI on the medial side (27) to calculate structural parameters, including bone volume/total volume fraction, trabecular number, and trabecular thickness via Scanco software for trabecular bone 3-dimensional standard microstructural analysis. In addition, meniscal ossicle bone volume was directly measured via Scanco software for standard microstructural analysis.

In vitro cartilage explant model. To assess the impact of decorin loss on sGAG release from degenerative cartilage, femoral head cartilage explants were isolated from 3-week-old WT and $\text{Dcn}^{-/-}$ mice ($n = 6$ per group), according to an established procedure (28). For live explants, immediately after harvesting, explants were sterilized and pre-cultured at 37°C with 5% CO_2 for 2 days in Dulbecco's Modified Eagle's Medium (catalog no. 11960; ThermoFisher) mixed with 10% fetal bovine serum, $1 \times$ insulin-transferin-selenium-sodium pyruvate (catalog no. 51300; ThermoFisher), 2 mM L-glutamine (catalog no. 25030; ThermoFisher), 250 μM L-ascorbic acid 2-phosphate (catalog no. A8960; Sigma), and $2 \times$ penicillin-streptomycin (catalog no. 15140; ThermoFisher). The explants were then cultured in the same media but with $1 \times$ penicillin-streptomycin, supplemented with 10 ng/ml recombinant murine interleukin-1 β (IL-1 β) (catalog no. 211-11B; PeproTech) for 3 days, with the control group cultured in the same manner but without IL-1 β . On day 3, the amounts of sGAGs released to the media and retained in cartilage were assessed via dimethylmethylene blue dye binding assay after papain digestion, and qPCR was performed on additional explants to measure the expression of anabolic and catabolic genes. Total RNA (250 ng per well) was subjected to reverse transcription using a TaqMan reverse transcription kit (catalog no. N8080234; ThermoFisher) with amplification carried out via PowerUp SYBR Green Master Mix (catalog no. A25742; ThermoFisher) on a RealPlex 4S Mastercycler (Eppendorf). The genes tested and their associated primer sequences are listed in Supplementary Table 1, available on the *Arthritis & Rheumatology* web site at <http://onlinelibrary.wiley.com/doi/10.1002/art.41254/abstract>.

For devitalized explants, after extraction and pre-culture, explants underwent 3 freeze-thaw cycles between -80°C for 2 hours and 37°C for 45 minutes (29), and were cultured in the same medium supplemented with 20 nM recombinant human ADAMTS-5 (a disintegrin and metalloproteinase with thrombospondin motifs 5) (30) (catalog no. 2198-AD; R&D Systems) or MMP-13 (31) (catalog no. 511-MM-010; R&D Systems) for 4

days. The amounts of sGAGs released to media and retained in explant were assessed according to the same procedure as described above. For both live and devitalized explants, cell viability was assessed via fluorescein diacetate and propidium iodide staining (Supplementary Figure 4, *Arthritis & Rheumatology* web site at <http://onlinelibrary.wiley.com/doi/10.1002/art.41254/abstract>) (29).

Statistical analysis. To avoid the assumption of normal distribution of the data, nonparametric statistical tests were applied. To test the significance between genotypes within each surgery type or treatment condition, Mann-Whitney U

test was applied to compare t_{total} , $t_{uncalcified}$, E_{ind} , modified Mankin score, micro-CT outcomes, gene expression, and ratio of sGAG release. Wilcoxon's signed rank test was applied to compare these parameters between surgery types within each genotype. To compare the degree of fibril alignment, θ , the Mardia and Jupp test of concentration equality (32) was used to compare the von Mises concentration parameter κ between genotypes and surgery types. All quantitative outcomes and statistical analysis results are summarized in Supplementary Tables 2–5, available on the *Arthritis & Rheumatology* web site at <http://onlinelibrary.wiley.com/doi/10.1002/art.41254/abstract>. For all tests, the significance level was set at $\alpha = 0.05$.

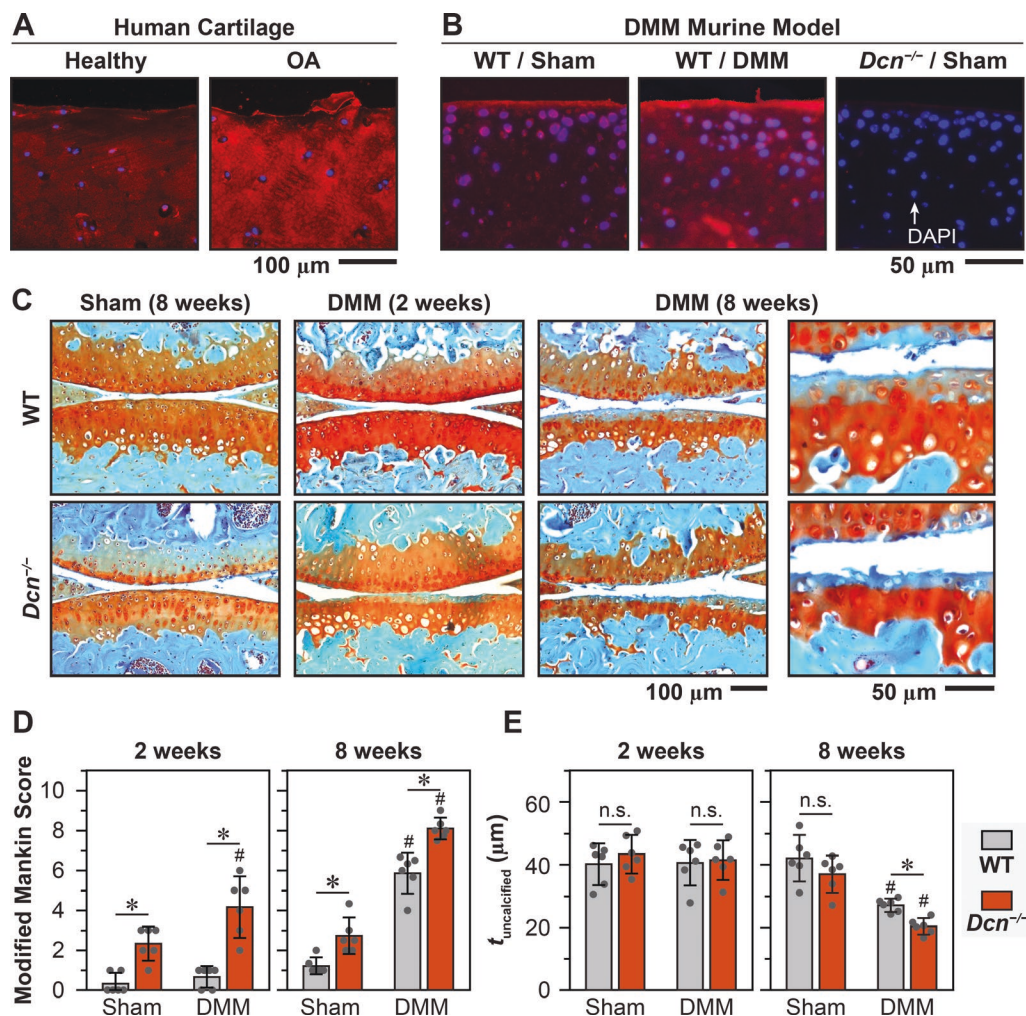


Figure 1. Accelerated progression of post-traumatic osteoarthritis (OA) in decorin-null ($Dcn^{-/-}$) mice after destabilization of the medial meniscus (DMM). **A** and **B**, Immunofluorescence images showing the up-regulation of decorin in human OA cartilage (**A**) and in wild-type (WT) murine knee cartilage 8 weeks after surgical DMM (**B**). Cartilage from Sham-operated $Dcn^{-/-}$ mice (DAPI stained [blue]) was used as a negative control. **C**, Representative images of Safranin O–Fast Green–stained cartilage specimens from WT and $Dcn^{-/-}$ mice 8 weeks after Sham surgery, 2 weeks after surgical DMM, and 8 weeks after surgical DMM. More severe cartilage damage was observed in the $Dcn^{-/-}$ mice. **D** and **E**, Modified Mankin score (**D**) and thickness of uncalcified cartilage ($t_{uncalcified}$) in the medial femoral condyle (**E**) in WT and $Dcn^{-/-}$ mice 2 weeks and 8 weeks after Sham surgery or surgical DMM. $Dcn^{-/-}$ mice had more severe OA than WT mice. Bars show the mean \pm 95% confidence interval. Circles indicate individual mice ($n = 6$ per group). * = $P < 0.05$; # = $P < 0.05$ versus Sham surgery for the same genotype. n.s. = not significant.

RESULTS

Accelerated cartilage degradation in $Dcn^{-/-}$ mice after surgical DMM. In healthy human cartilage matrix, decorin was present in both the pericellular and further-removed territorial/interterritorial domains of the ECM (Figure 1A). In human OA specimens, decorin was significantly up-regulated and present throughout the damaged cartilage matrix. This observation was consistent with the findings of previous studies showing an increase in decorin in human OA cartilage (14,15). In WT mice subjected to Sham surgery, decorin was also distributed throughout the ECM. By 8 weeks after surgical DMM, we detected increased staining of decorin in WT mouse cartilage (Figure 1B), which validated DMM as an appropriate model for investigating the role of decorin and its up-regulation in post-traumatic OA.

In the DMM model, $Dcn^{-/-}$ mice developed accelerated cartilage degradation compared to WT mice, as shown by histological analysis (Figure 1C). Two weeks after surgery, while WT mouse cartilage did not show appreciable damage, $Dcn^{-/-}$ mouse cartilage

started to develop loss of sGAG staining on the surface, contributing to higher modified Mankin scores (Figure 1D). By 8 weeks after surgery, both genotypes exhibited salient OA signs, which were more pronounced in $Dcn^{-/-}$ mice. Specifically, $Dcn^{-/-}$ mouse cartilage was characterized by the formation of surface fissures, a further reduction in sGAG staining, more substantial cartilage thinning (lower $t_{uncalcified}$) (Figure 1E), and thus, significantly higher Mankin scores (Figure 1D).

Development of pronounced collagen fibrillation on the cartilage surface in $Dcn^{-/-}$ mice after surgical DMM.

One distinctive OA phenotype of $Dcn^{-/-}$ mouse cartilage was the nanoscale surface fibrillation, as observed by scanning electron microscopy (Figure 2A). In healthy joints, the cartilage surface is covered by a transversely random mesh of collagen fibrils (33), present in both WT and $Dcn^{-/-}$ adult mouse cartilage (Supplementary Figure 3, available on the *Arthritis & Rheumatology* web site at <http://onlinelibrary.wiley.com/doi/10.1002/art.41254/abstract>) (9). In the Sham-operated groups, both genotypes retained this random

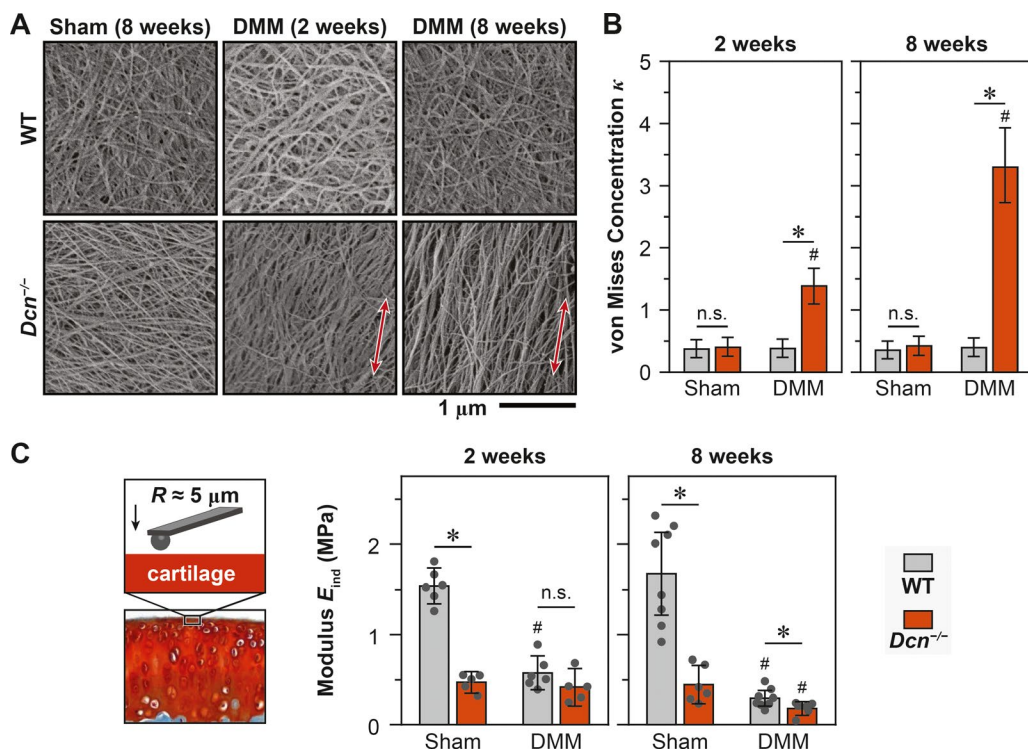


Figure 2. Pronounced cartilage surface fibrillation in decorin-null ($Dcn^{-/-}$) mice subjected to surgical destabilization of the medial meniscus (DMM). **A**, Representative scanning electron microscopy images showing the nanostructure of collagen fibrils on condyle cartilage surfaces in wild-type (WT) and $Dcn^{-/-}$ mice 8 weeks after Sham surgery, 2 weeks after surgical DMM, and 8 weeks after surgical DMM. **Arrows** show the mediolateral direction. **B**, Degree of fibril alignment, measured by the von Mises concentration parameter κ , in WT and $Dcn^{-/-}$ mouse cartilage 2 weeks and 8 weeks after Sham surgery or surgical DMM. The cartilage surface in $Dcn^{-/-}$ mice had a significantly higher von Mises concentration than that in WT mice after surgical DMM. Bars show the mean \pm 95% confidence interval (95% CI) estimated from ≥ 300 fibrils pooled from 4 animals per group. **C**, Cartilage tissue modulus measured on the medial condyles in WT mice and $Dcn^{-/-}$ mice by atomic force microscopy–nanoindentation. Left, Illustration of the measurement of cartilage tissue modulus. Right, Cartilage tissue effective indentation modulus (E_{ind}) in WT and $Dcn^{-/-}$ mice 2 weeks and 8 weeks after Sham surgery or surgical DMM. Bars show the mean \pm 95% CI ($n = 5$ or more mice per group). Circles represent the mean value from 10 or more locations measured in 1 animal. * = $P < 0.05$; # = $P < 0.05$ versus Sham surgery for the same genotype. n.s. = not significant. Color figure can be viewed in the online issue, which is available at <http://onlinelibrary.wiley.com/doi/10.1002/art.41254/abstract>.

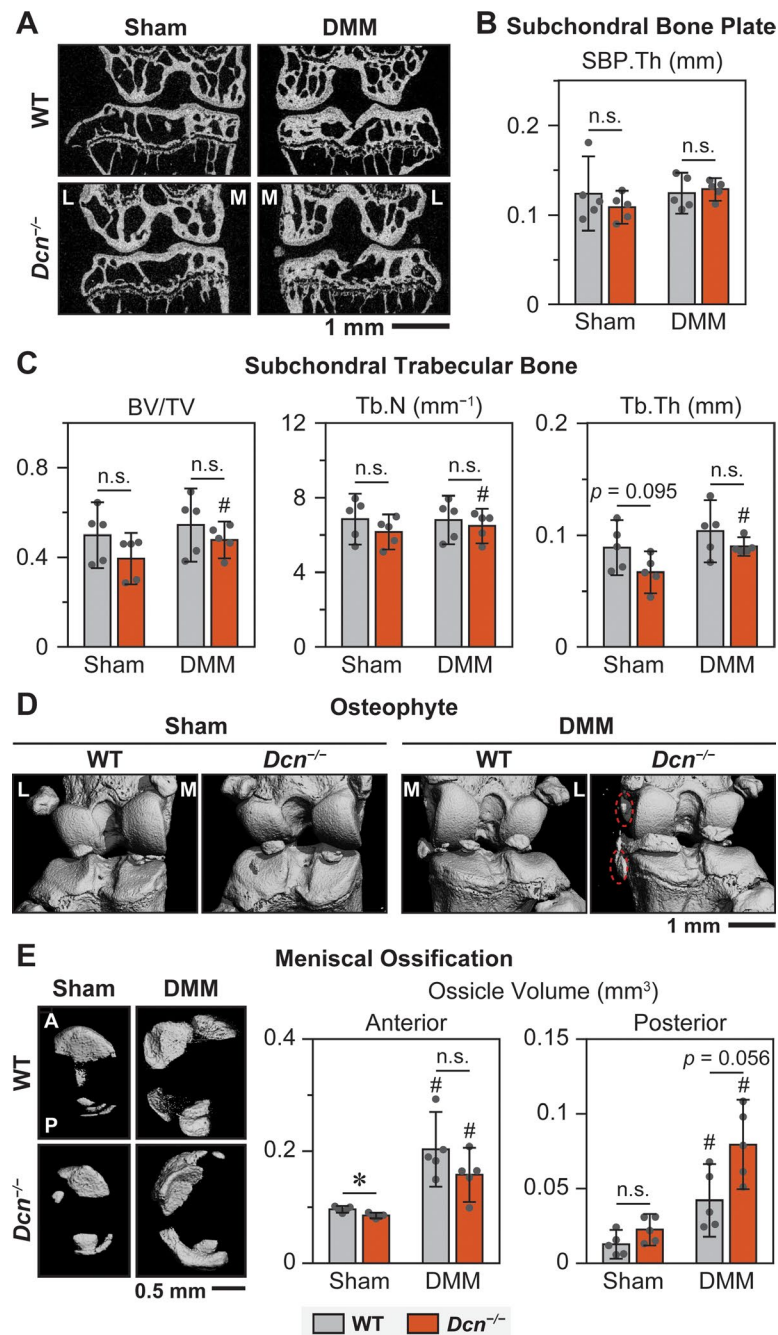


Figure 3. Comparison of subchondral bone structure in wild-type (WT) and decorin-null (*Dcn*^{-/-}) mice 8 weeks after surgery. **A**, Representative 2-dimensional micro-computed tomography (micro-CT) frontal plane images of the knee joint in WT and *Dcn*^{-/-} mice 8 weeks after Sham surgery or surgical destabilization of the medial meniscus (DMM). L = lateral; M = medial. **B** and **C**, Subchondral bone plate thickness (SBP.Th) (**B**) and subchondral trabecular bone structural parameters (**C**) of the medial tibia in WT and *Dcn*^{-/-} mice 8 weeks after Sham surgery or surgical DMM, analyzed on micro-CT images. BV/TV = bone volume/total volume; Tb.N = trabecular number; Tb.Th = trabecular thickness. **D**, Representative reconstructed 3-dimensional (3-D) micro-CT images showing the presence of osteophytes (encircled) in *Dcn*^{-/-} mice 8 weeks after DMM but not in other groups. **E**, Meniscal ossification. Left, Representative reconstructed 3-D micro-CT images (top view) of medial meniscal ossicles showing increased ossification 8 weeks after DMM in both mouse genotypes. A = anterior; P = posterior. Right, Medial meniscal ossicle volume at both the anterior and posterior ends in WT and *Dcn*^{-/-} mice 8 weeks after Sham surgery or surgical DMM. In **B**, **C**, and the right panel of **E**, bars show the mean \pm 95% confidence interval ($n = 5$ mice per group). Circles represent the mean value from 10 or more locations measured in 1 animal. * = $P < 0.05$; # = $P < 0.05$ versus Sham surgery for the same genotype. P values are shown on the figure in cases where a trend ($P < 0.10$) was detected. n.s. = not significant.

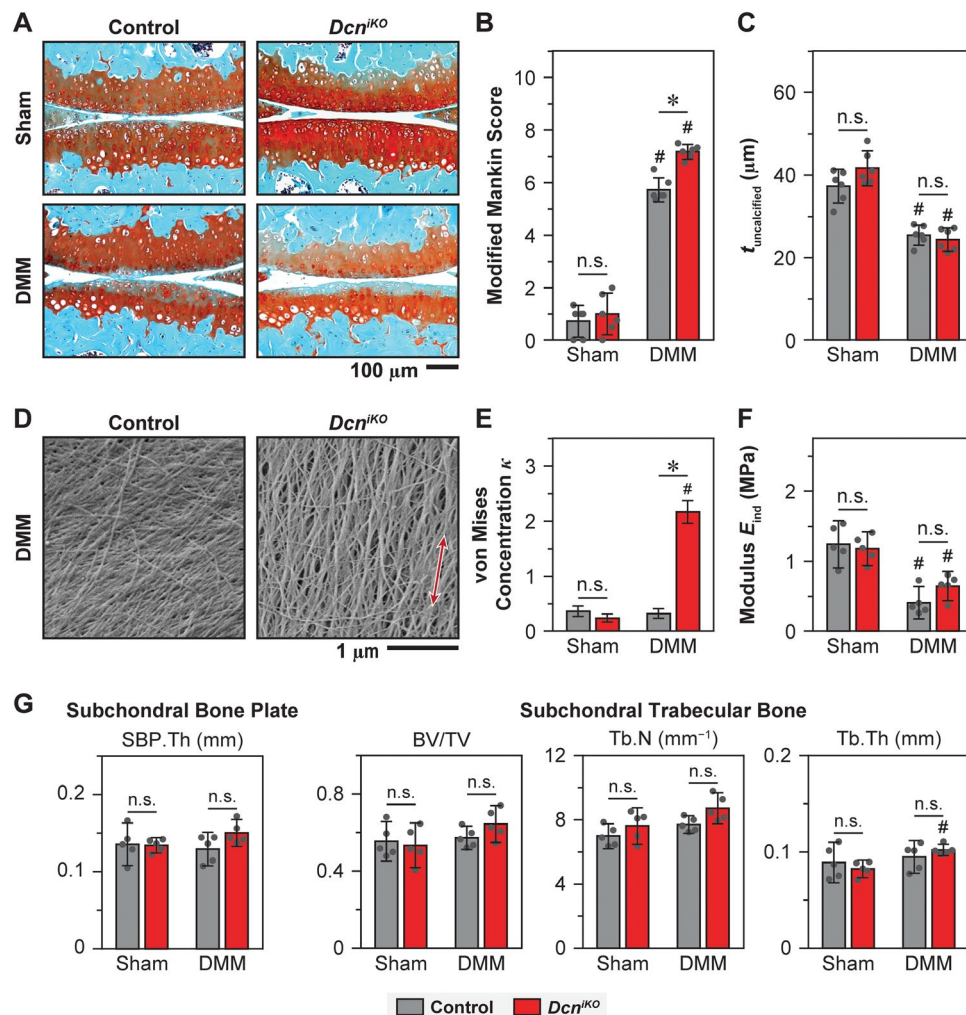


Figure 4. Accelerated progression of post-traumatic osteoarthritis (OA) 8 weeks after surgical destabilization of the medial meniscus (DMM) in mice with decorin deleted at the time of surgery (inducible decorin-knockout [Dcn^{IKO}] mice). **A**, Representative images of Safranin O–Fast Green–stained cartilage specimens from control mice and Dcn^{IKO} mice 8 weeks after Sham surgery or surgical DMM. More severe cartilage damage was observed in the Dcn^{IKO} mice. **B** and **C**, Modified Mankin score (**B**) and thickness of uncalcified cartilage ($t_{\text{uncalcified}}$) in the medial femoral condyle (**C**) in control and Dcn^{IKO} mice 8 weeks after Sham surgery or surgical DMM. Dcn^{IKO} mice had more severe OA than control mice. **D**, Representative scanning electron microscopy images showing the nanostructure of collagen fibrils on condyle cartilage surfaces in control and Dcn^{IKO} mice 8 weeks after DMM. Arrow shows the mediolateral direction. **E**, Degree of fibril alignment, measured by the von Mises concentration parameter κ , in control and Dcn^{IKO} mice 8 weeks after Sham surgery or surgical DMM. The cartilage surface in Dcn^{IKO} mice had a significantly higher von Mises concentration than that in control mice after surgical DMM. Results are from ≥ 300 fibrils pooled from 4 animals per group. **F**, Cartilage tissue effective indentation modulus (E_{ind}) measured on the medial condyles in control and Dcn^{IKO} mice by atomic force microscopy–nanoindentation 8 weeks after Sham surgery or surgical DMM. **G**, Subchondral bone plate thickness (SBP.Th) and subchondral trabecular bone structural parameters of the medial tibia in control and Dcn^{IKO} mice 8 weeks after Sham surgery or surgical DMM, analyzed on micro–computed tomography images. BV/TV = bone volume/total volume; Tb.N = trabecular number; Tb.Th = trabecular thickness. Bars in **B**, **C**, **E**, **F**, and **G** show the mean \pm 95% confidence interval ($n = 6$ mice per group in **B** and **C**, 4 mice per group in **E**, and 5 mice per group in **F** and **G**). Circles represent the mean value from 10 or more locations measured in 1 animal. * = $P < 0.05$; # = $P < 0.05$ versus Sham surgery for the same genotype. n.s. = not significant. Color figure can be viewed in the online issue, which is available at <http://onlinelibrary.wiley.com/doi/10.1002/art.41254/abstract>.

fibrillar architecture. In the surgical DMM groups, this feature was retained in WT mice up to 8 weeks after surgery. In contrast, Dcn^{IKO} mouse cartilage surface started to develop aligned fibrils as early as 2 weeks after surgery, and were dominated by highly aligned, densely packed collagen fibrils 8 weeks after surgery. These changes were signified by the much higher von Mises concentration, κ , in Dcn^{IKO} mouse cartilage (Figure 2B). These fibrils

were aligned along the mediolateral orientation (Supplementary Figure 3), suggesting that the surface fibrillation could be induced by extensive shearing of the destabilized medial meniscus during joint loading. In both genotypes, cartilage damage was associated with marked reduction in modulus (E_{ind}) (Figure 2C). This reduction was attributed to the loss of cartilage ECM structural integrity and illustrated the impaired cartilage load-bearing function in OA (23). In

both the Sham-operated group and the group subjected to surgical DMM, $Dcn^{-/-}$ mouse cartilage showed lower modulus compared to WT mouse cartilage, suggesting that loss of decorin impairs cartilage load-bearing function both during normal skeletal growth and in DMM-induced cartilage degradation.

Lack of an appreciable subchondral bone phenotype in $Dcn^{-/-}$ mice after surgical DMM. Given the crucial interplay between cartilage and subchondral bone in OA development (2), we investigated whether loss of decorin also impacted subchondral bone after DMM. Eight weeks after surgery, for both mouse genotypes, the DMM group showed no significant structural changes in either the subchondral bone plate or STB relative to the Sham-operated group (Figures 3A–C). This observation is consistent with the findings of previous studies showing that in the DMM model, subchondral bone changes occur only after the erosion of cartilage in late OA (34). No differences were detected between the WT and $Dcn^{-/-}$ mice with regard to subchondral bone plate or STB structure in either the group subjected to DMM or the Sham-operated group, indicating that loss of decorin does not impact the remodeling of subchondral bone in the DMM model. In contrast, 8 weeks after surgical DMM, we detected the formation of osteophytes in $Dcn^{-/-}$, but not WT, mouse joints (Figure 3D), which indicated more advanced OA (35). DMM increased meniscal ossification at the horns in both genotypes, and $Dcn^{-/-}$ mouse joints showed a marginally higher degree of ossification at the posterior, but not the anterior, end compared to WT mouse joints (Figure 3E). Taken together, micro-CT findings suggest that the accelerated OA progression in $Dcn^{-/-}$ mice is more likely to be a direct impact of decorin loss in cartilage, rather than a secondary effect arising from changes in underlying subchondral bone.

Acceleration of OA progression by ablation of decorin in Dcn^{iKO} mice at the time of DMM. The more severe OA phenotype in $Dcn^{-/-}$ mice could be attributed to both altered OA pathology and impaired joint growth prior to surgery in the absence of decorin. In the Sham-operated group, $Dcn^{-/-}$ mouse cartilage showed moderate Mankin scores (Figure 1D) and lower modulus relative to WT mice (Figure 2C), which was due to the lower sGAG content in $Dcn^{-/-}$ mouse cartilage even without surgery (9). To separate the role of decorin in OA from its role in joint growth, we studied OA progression in Dcn^{iKO} mice 8 weeks after surgery. The expression of decorin was maintained up to maturity, and only ablated at the time of DMM. In these mice, we also detected accelerated OA, with features comparable to those seen in $Dcn^{-/-}$ mice. Compared to control mice, Dcn^{iKO} mice developed higher Mankin scores, more pronounced reduction in sGAG staining, and salient surface fibrillation (Figures 4A–E). Dcn^{iKO} mice also developed osteophytes (Supplementary Figure 5, available on the *Arthritis & Rheumatology* web site at <http://onlinelibrary.wiley.com/doi/10.1002/art.41254/abstract>) but did not show appreciable subchondral

bone phenotype (Figure 4G). Thus, the accelerated OA phenotype in $Dcn^{-/-}$ mice and Dcn^{iKO} mice was primarily due to the loss of the protective role of decorin in DMM-induced cartilage degradation.

In comparison to $Dcn^{-/-}$ mice (Figures 1C–E), Dcn^{iKO} mice did not demonstrate more severe cartilage thinning (Figure 4C) and had moderately lower Mankin scores (Figure 4B). This confirmed that the OA phenotype in $Dcn^{-/-}$ mice was a result of the combined effects of both altered OA pathology and impaired joint growth. Further, while the modulus of Dcn^{iKO} cartilage was also reduced by DMM, it was similar to that of control mouse cartilage (Figure 4F) and higher than that of $Dcn^{-/-}$ mouse cartilage. The modulus of Dcn^{iKO} cartilage could reflect the properties of newly formed fibrous tissues on the surface, which lack aggrecan and associated sGAGs, and thus are incapable of dissipating energy through poroelasticity as normal hyaline cartilage.

Acceleration of aggrecan release from degenerative murine cartilage explants with the loss of decorin.

To determine if loss of decorin directly impacts chondrocyte catabolism, we analyzed chondrocyte gene expression in mouse femoral head cartilage explants (Figure 5A). Upon stimulation with IL-1 β , there was a decrease in the expression of the anabolic genes *Acan* and *Col2a1* in WT but not $Dcn^{-/-}$ mouse cartilage explants (Figure 5A). In contrast, major catabolic genes, including aggrecanases and MMPs, were significantly up-regulated by 10–100-fold after IL-1 β stimulation in both mouse genotypes. We did not detect significant differences between the 2 genotypes in any of the genes tested except for decorin. This suggests that decorin does not directly regulate the anabolic or catabolic activities of chondrocytes, either with or without IL-1 β stimulation.

Finally, we compared the amount of sGAGs released from explants in both live and devitalized conditions. $Dcn^{-/-}$ mouse cartilage has lower amounts of aggrecan and sGAGs than WT mouse cartilage, which indicates a lower concentration gradient for diffusion-driven release of sGAGs. Despite this, in live explants, when IL-1 β aggravated chondrocyte catabolism, a greater proportion of sGAGs was released from $Dcn^{-/-}$ mouse explants than from WT mouse explants (Figure 5B). Further, in devitalized explants, when chondrocyte metabolism was abolished, $Dcn^{-/-}$ mouse explants still experienced a higher degree of sGAG release upon exogenous proteolysis of aggrecan by ADAMTS-5 or MMP-13 (Figure 5C). Therefore, in the explant model, the absence of decorin accelerates the loss of fragmented aggrecan from cartilage matrix, but does not directly alter chondrocyte metabolism when stimulated with IL-1 β .

DISCUSSION

This study highlights the crucial role of decorin in mediating cartilage degradation in post-traumatic OA, as evidenced by the accelerated OA phenotype in both $Dcn^{-/-}$ and Dcn^{iKO} mice (Figures 1–4). We hypothesize that in degenerative cartilage,

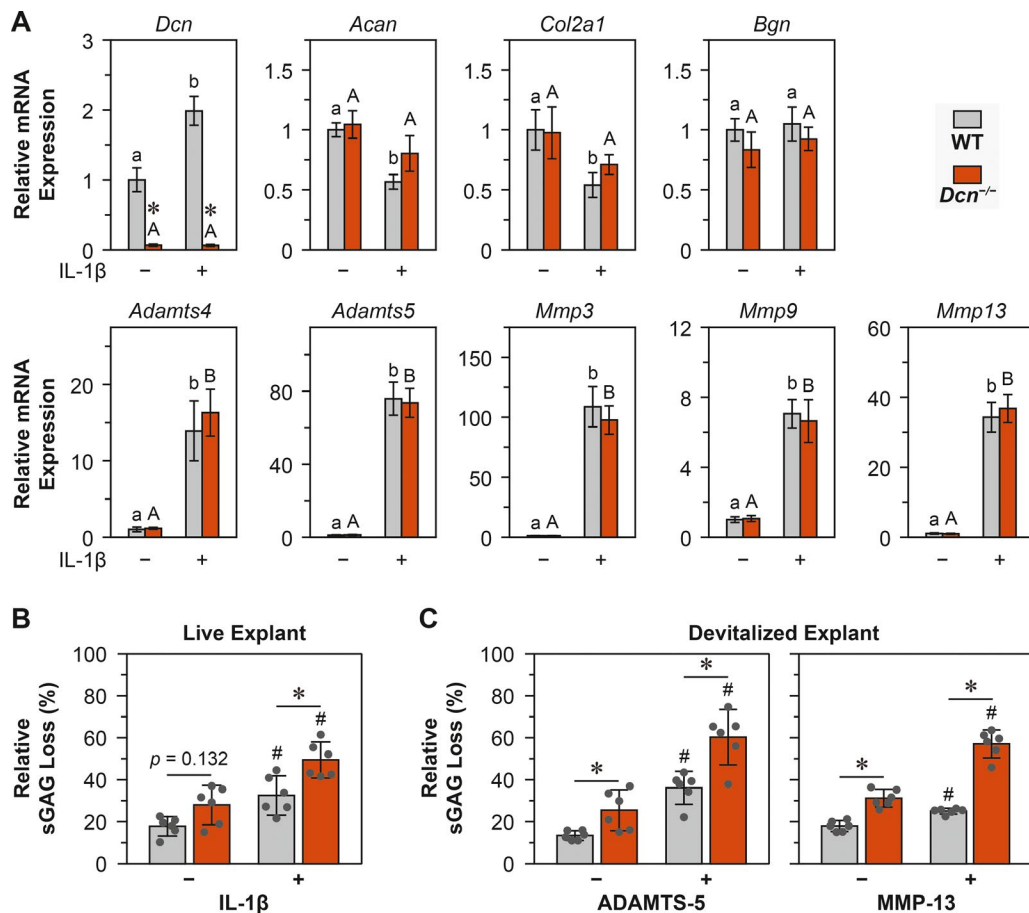


Figure 5. Loss of decorin accelerates the release of sulfated glycosaminoglycans (sGAGs) from degenerative murine cartilage explants but does not alter chondrocyte anabolism or catabolism. **A**, Expression of anabolic and catabolic genes by chondrocytes in femoral head cartilage explants from wild-type (WT) and decorin-null (*Dcn*^{-/-}) mice, cultured in Dulbecco's Modified Eagle's Medium (DMEM) for 3 days and left unstimulated or stimulated with the inflammatory cytokine interleukin-1 β (IL-1 β). Expression was measured by quantitative polymerase chain reaction. Bars show the mean \pm SEM ($n = 6$ samples per group). * = $P < 0.01$ versus WT mice. Different letters indicate significant differences between the untreated and IL-1 β -treated groups within each genotype. **B**, Relative percentage of sGAGs released from live murine cartilage explants cultured in DMEM for 3 days and left unstimulated or stimulated with IL-1 β , measured by dimethylmethylene blue (DMMB) dye binding assay. **C**, Relative percentage of sGAGs released from devitalized murine cartilage explants cultured in DMEM for 4 days and left unstimulated or stimulated by a disintegrin and metalloproteinase with thrombospondin motifs 5 (ADAMTS-5) or matrix metalloproteinase 13 (MMP-13), measured by DMMB dye binding assay. In **B** and **C**, bars show the mean \pm 95% confidence interval ($n = 6$ samples per group). Circles represent the value from 1 biologic repeat. * = $P < 0.05$; # = $P < 0.05$ versus untreated samples from the same genotype. Color figure can be viewed in the online issue, which is available at <http://onlinelibrary.wiley.com/doi/10.1002/art.41254/abstract>.

decorin increases the retention of fragmented aggrecan within degrading matrix, thereby delaying aggrecan loss and cartilage damage (Figure 6A). This hypothesis extends findings from our recent study on the regulatory roles of decorin in postnatal cartilage growth (9). Specifically, we showed that in healthy cartilage, decorin functions as a "physical linker" (Figure 6B) to increase molecular adhesion of aggrecan-aggrecan and aggrecan-type II collagen fibrils. The canonical assembly mechanism of the aggrecan network in the ECM is the aggregation of aggrecan-HA via the G1 domain (36), but this mechanism does not fully explain the integrity of aggrecan across development and disease states (37). While aggrecan can also form networks through interacting with tenascins (38) and fibulin -2 (39) via its G3 domain,

the presence of G3 domain decreases markedly with age (40). To this end, the decorin-mediated aggrecan network assembly could be a crucial mechanism in maintaining the integrity of the aggrecan network in the ECM; this notion is supported by the markedly impaired biomechanical functions of *Dcn*^{-/-} mouse cartilage (9). In OA, when aggrecan molecules become increasingly fragmented and dissociated from the aggrecan-HA aggregates (4), the up-regulation of decorin could be a reparative attempt to increase the retention of fragmented aggrecan, and so, attenuate aggrecan depletion (Figure 6A). Indeed, this hypothesis is supported by outcomes from explant models, in which loss of decorin accelerates the release of fragmented aggrecan from both live and devitalized cartilage (Figures 5B and C).

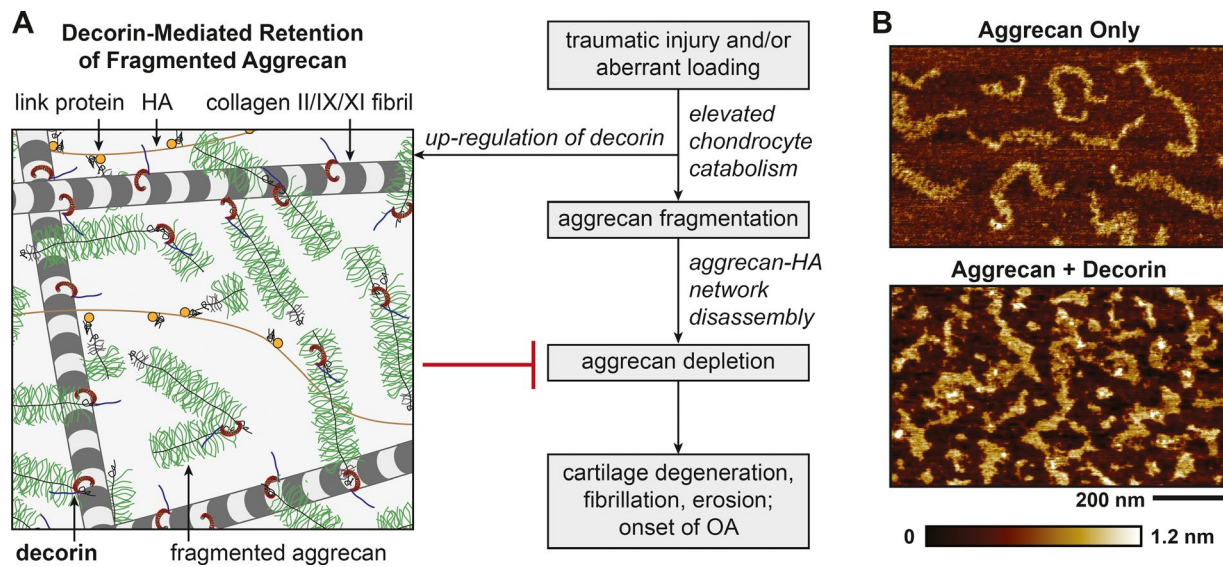


Figure 6. **A**, Schematic illustration of the working hypothesis on the structural role of decorin in degenerative cartilage matrix. Left, Binding of decorin to aggrecan, increasing the adhesion of aggrecan to other aggrecan molecules and to type II/IX/XI collagen fibrils, thereby enhancing the retention of fragmented aggrecan in the extracellular matrix. Right, Flow diagram showing the compensatory effects of decorin up-regulation to slow down the depletion of aggrecan, and thus, attenuate cartilage degradation and the onset of osteoarthritis (OA). **B**, Illustration of the role of decorin in increasing the aggregation of aggrecan. Tapping mode atomic force microscopy images show that aggrecan molecules remain as individual monomers when reconstituted on mica surface *in vitro*, but form interconnected networks with the addition of free decorin protein. HA = hyaluronan. Adapted, with permission, from ref. 9. Color figure can be viewed in the online issue, which is available at <http://onlinelibrary.wiley.com/doi/10.1002/art.41254/abstract>

In the DMM model, both $Dcn^{-/-}$ and Dcn^{iKO} mouse cartilage develop extensive surface fibrillation (Figures 2A and B and Figures 4D and E). We attribute this effect to the loss of the protective effect of aggrecan against collagen remodeling. In the ECM, the densely packed, aggrecan–HA aggregates occupy the ~100-nm–sized interfibrillar spacing within the porous type II/IX/XI collagen network (41), limiting aberrant collagen fibril lateral fusion and overgrowth. When loss of decorin leads to accelerated aggrecan depletion and impairs aggrecan's protection of the collagen fibrillar network following DMM, the extensive shear and frictional forces from the destabilized meniscus can induce the alignment of collagen fibrils along the shear direction (Figures 2A and 4D). In addition, decorin could also directly inhibit fibril lateral fusion given its capability of binding to type II collagen (42), but such contribution may be less important given its low mass concentration relative to aggrecan in cartilage (13). The presence of aligned fibrils suggests that hyaline cartilage loses its integrity and transforms into fibrocartilage, which does not possess the energy dissipation function endowed by aggrecan (8). These results thus support the notion of a critical protective role of decorin in inhibiting cartilage fibrillation, an irreversible degenerative step in OA progression (8).

Integrating this study with our recent work on young adult $Dcn^{-/-}$ mouse cartilage (9), we show that in both healthy and degenerative cartilage, the primary role of decorin is to mediate ECM assembly, rather than to influence chondrocyte metabolism. The absence of the impact of decorin on chondrocyte response to IL-1 β (Figure 5A) is similar to its lack of impact on the response

to growth factor TGF β 1 (9). In both scenarios, although loss of decorin does not alter chondrocyte metabolism, it significantly reduces the retention of aggrecan in cartilage matrix, both during degeneration *in situ* (Figures 5B and C) and during regeneration in alginate culture (9). *In vivo*, the role of decorin in increasing aggrecan retention could be more crucial, as the extensive physiologic joint loading and associated interstitial fluid flow can further promote aggrecan depletion when its assembly is impaired. This finding is different from previous studies showing higher resistance of $Dcn^{-/-}$ mice to forced exercise-induced OA (18). We attribute this contrast mainly to differences in the OA models used. The forced exercise model represents joint overuse (43), while DMM induces joint instability and inflammation (19), and so the two models could have different disease etiology. For example, in WT mouse cartilage, the expression of decorin is suppressed by forced exercise (18), but elevated by DMM (Figure 1B). This increase in decorin expression corroborates observations in both murine (Figure 5A) and bovine (44) cartilage explants stimulated with IL-1 β , as well as cartilage specimens from OA patients (14,15). To this end, the protective role of decorin in post-traumatic OA is confirmed by the consistency of an accelerated OA phenotype in $Dcn^{-/-}$ and Dcn^{iKO} mice (Figures 1–4), which were established in different manners (20,21).

This study has several limitations. First, while we showed that decorin increases molecular adhesion of aggrecan (9), we did not identify how decorin specifically interacts with aggrecan core protein or its sGAGs, and how such interaction is altered when decorin

becomes increasingly fragmented as OA advances (45–47). To address this limitation, our ongoing studies sought to test the interactions between purified decorin, aggrecan, and type II collagen at the single-molecule level. Second, the half-life of decorin in adult murine cartilage is unknown. The lack of phenotype in the Sham-operated *Dcn*^{IKO} mice (Figure 4) is in stark contrast with the pronounced phenotype that resulted from induced decorin knockout at 1 month of age (9). This could be due to either the presence of residual decorin, or the fact that decorin plays a less essential role in adulthood (≥ 3 months of age). However, while we cannot delineate the influence of residual decorin in DMM, the accelerated OA phenotype in *Dcn*^{IKO} mice (Figure 4) clearly demonstrated the impact of ablating the decorin up-regulation on DMM-induced cartilage degradation. Third, although we showed that decorin does not significantly impact chondrocyte catabolism under stimulation with IL-1 β , given its versatile interactomes (10), it is possible that decorin may affect chondrocyte signaling through its bindings with cell surface receptors and cytokines in other OA models. For example, spontaneous OA is associated with reduced autophagy in cartilage (48), and decorin may also ameliorate OA through evoking autophagy (49), which will be a topic of our future work.

In summary, this study identifies decorin as a central player in cartilage degradation in post-traumatic OA. Loss of decorin aggravates aggrecan depletion and surface fibrillation, leading to accelerated cartilage damage. We hypothesize that up-regulation of decorin in early OA acts as a reparative attempt to increase the retention of fragmented aggrecan in the ECM, thereby delaying aggrecan loss, cartilage fibrillation, and irreversible cartilage breakdown (Figure 6A). This role is mediated by the interactions of decorin with aggrecan molecules and type II collagen fibrils. Therefore, modulating decorin activities through decorin-targeting gene therapies or decorin-based biomaterials has the potential to attenuate OA progression and prolong joint use.

ACKNOWLEDGMENTS

We thank Dr. L. W. Fisher (National Institute of Dental and Craniofacial Research, Bethesda, MD) for the generous gift of decorin antibodies and Dr. S. Wakitani (Hiroshima University, Hiroshima, Japan) for kindly providing human articular cartilage sections.

AUTHOR CONTRIBUTIONS

All authors were involved in drafting the article or revising it critically for important intellectual content, and all authors approved the final version to be published. Dr. Lin Han had full access to all of the data in the study and takes responsibility for the integrity of the data and the accuracy of the data analysis.

Study conception and design. Li, B. Han, Birk, L. Han.

Acquisition of data. Li, B. Han, Wang, Tong, Wei, Tseng, Liu, Enomoto-Iwamoto, Qin, Birk, L. Han.

Analysis and interpretation of data. Li, B. Han, Wang, Tong, Wei, Tseng, L.-H. Han, Liu, Enomoto-Iwamoto, Mauck, Qin, Iozzo, Birk, L. Han.

REFERENCES

1. Helmick CG, Felson DT, Lawrence RC, Gabriel S, Hirsch R, Kwoh CK, et al. Estimates of the prevalence of arthritis and other rheumatic conditions in the United States: part I. *Arthritis Rheum* 2008;58:15–25.
2. Goldring MB, Goldring SR. Articular cartilage and subchondral bone in the pathogenesis of osteoarthritis. *Ann N Y Acad Sci* 2010;1192:230–7.
3. Roughley PJ, Mort JS. The role of aggrecan in normal and osteoarthritic cartilage [review]. *J Exp Orthop* 2014;1:8.
4. Lohmander LS, Neame PJ, Sandy JD. The structure of aggrecan fragments in human synovial fluid: evidence that aggrecanase mediates cartilage degradation in inflammatory joint disease, joint injury, and osteoarthritis. *Arthritis Rheum* 1993;36:1214–22.
5. Krishnan Y, Grodzinsky AJ. Cartilage diseases. *Matrix Biol* 2018;71–2:51–69.
6. Guilak F, Nims RJ, Dicks A, Wu CL, Meulenbelt I. Osteoarthritis as a disease of the cartilage pericellular matrix. *Matrix Biol* 2018;71–2:40–50.
7. Pratta MA, Yao W, Decicco C, Tortorella MD, Liu R-Q, Copeland RA, et al. Aggrecan protects cartilage collagen from proteolytic cleavage. *J Biol Chem* 2003;278:45539–45.
8. Stoop R, Buma P, van der Kraan PM, Hollander AP, Billingham RC, Meijers TH, et al. Type II collagen degradation in articular cartilage fibrillation after anterior cruciate ligament transection in rats. *Osteoarthritis Cartilage* 2001;9:308–15.
9. Han B, Li Q, Wang C, Patel P, Adams SM, Doyran B, et al. Decorin regulates the aggrecan network integrity and biomechanical functions of cartilage extracellular matrix. *ACS Nano* 2019;13:11320–33.
10. Gubbiotti MA, Vallet SD, Ricard-Blum S, Iozzo RV. Decorin interacting network: a comprehensive analysis of decorin-binding partners and their versatile functions. *Matrix Biol* 2016;55:7–21.
11. Chen S, Birk DE. The regulatory roles of small leucine-rich proteoglycans in extracellular matrix assembly. *FEBS J* 2013;280:2120–37.
12. McAlinden A, Dudhia J, Bolton MC, Lorenzo P, Heinegård D, Bayliss MT. Age-related changes in the synthesis and mRNA expression of decorin and aggrecan in human meniscus and articular cartilage. *Osteoarthritis Cartilage* 2001;9:33–41.
13. Poole AR, Rosenberg LC, Reiner A, Ionescu M, Bogoch E, Roughley PJ. Contents and distributions of the proteoglycans decorin and biglycan in normal and osteoarthritic human articular cartilage. *J Orthop Res* 1996;14:681–9.
14. Cs-Szabó G, Roughley PJ, Plaas AH, Glant TT. Large and small proteoglycans of osteoarthritic and rheumatoid articular cartilage. *Arthritis Rheum* 1995;38:660–8.
15. Cs-Szabó G, Melching LI, Roughley PJ, Glant TT. Changes in messenger RNA and protein levels of proteoglycans and link protein in human osteoarthritic cartilage samples. *Arthritis Rheum* 1997;40:1037–45.
16. Barreto G, Soininen A, Ylinen P, Sandelin J, Konttinen YT, Nordstrom DC, et al. Soluble biglycan: a potential mediator of cartilage degradation in osteoarthritis. *Arthritis Res Ther* 2015;17:379.
17. Ni GX, Li Z, Zhou YZ. The role of small leucine-rich proteoglycans in osteoarthritis pathogenesis. *Osteoarthritis Cartilage* 2014;22:896–903.
18. Gronau T, Kruger K, Prein C, Aszodi A, Gronau I, Iozzo RV, et al. Forced exercise-induced osteoarthritis is attenuated in mice lacking the small leucine-rich proteoglycan decorin. *Ann Rheum Dis* 2017;76:442–9.
19. Glasson SS, Blanchet TJ, Morris EA. The surgical destabilization of the medial meniscus (DMM) model of osteoarthritis in the 129/SvEv mouse. *Osteoarthritis Cartilage* 2007;15:1061–9.

20. Danielson KG, Baribault H, Holmes DF, Graham H, Kadler KE, Iozzo RV. Targeted disruption of decorin leads to abnormal collagen fibril morphology and skin fragility. *J Cell Biol* 1997;136:729–43.
21. Robinson KA, Sun M, Barnum CE, Weiss SN, Huegel J, Shetye SS, et al. Decorin and biglycan are necessary for maintaining collagen fibril structure, fiber realignment, and mechanical properties of mature tendons. *Matrix Biol* 2017;64:81–93.
22. McNulty MA, Loeser RF, Davey C, Callahan MF, Ferguson CM, Carlson CS. Histopathology of naturally occurring and surgically induced osteoarthritis in mice. *Osteoarthritis Cartilage* 2012;20:949–56.
23. Doyran B, Tong W, Li Q, Jia H, Zhang X, Chen C, et al. Nanoindentation modulus of murine cartilage: a sensitive indicator of the initiation and progression of post-traumatic osteoarthritis. *Osteoarthritis Cartilage* 2017;25:108–17.
24. Wang C, Brisson BK, Terajima M, Li Q, Hoxha K, Han B, et al. Type III collagen is a key regulator of the collagen fibrillar structure and biomechanics of articular cartilage and meniscus. *Matrix Biol* 2020;85–6:47–67.
25. Li Q, Qu F, Han B, Wang C, Li H, Mauck RL, et al. Micromechanical anisotropy and heterogeneity of the meniscus extracellular matrix. *Acta Biomater* 2017;54:356–66.
26. Huang H, Skelly JD, Ayers DC, Song J. Age-dependent changes in the articular cartilage and subchondral bone of C57BL/6 mice after surgical destabilization of medial meniscus. *Sci Rep* 2017;7:42294.
27. Moodie JP, Stok KS, Muller R, Vincent TL, Shefelbine SJ. Multimodal imaging demonstrates concomitant changes in bone and cartilage after destabilisation of the medial meniscus and increased joint laxity. *Osteoarthritis Cartilage* 2011;19:163–70.
28. Stanton H, Golub SB, Rogerson FM, Last K, Little CB, Fosang AJ. Investigating ADAMTS-mediated aggrecanolytic activity in mouse cartilage. *Nat Protoc* 2011;6:388–404.
29. Clements KM, Bee ZC, Crossingham GV, Adams MA, Sharif M. How severe must repetitive loading be to kill chondrocytes in articular cartilage? *Osteoarthritis Cartilage* 2001;9:499–507.
30. Seuffert F, Weidner D, Baum W, Schett G, Stock M. Upper zone of growth plate and cartilage matrix associated protein protects cartilage during inflammatory arthritis. *Arthritis Res Ther* 2018;20:88.
31. Rojas FP, Batista MA, Lindburg CA, Dean D, Grodzinsky AJ, Ortiz C, et al. Molecular adhesion between cartilage extracellular matrix macromolecules. *Biomacromolecules* 2014;15:772–80.
32. Mardia KV, Jupp PE. Tests of von Mises distributions. In: *Directional Statistics*. London: John Wiley & Sons, Ltd.; 2000. p. 119–43.
33. Vanden Berg-Foels WS, Scipioni L, Huynh C, Wen X. Helium ion microscopy for high-resolution visualization of the articular cartilage collagen network. *J Microsc* 2012;246:168–76.
34. Jia H, Ma X, Wei Y, Tong W, Tower RJ, Chandra A, et al. Loading-induced reduction in Sclerostin as a mechanism of subchondral bone plate sclerosis in mouse knee joints during late-stage osteoarthritis. *Arthritis Rheumatol* 2018;70:230–41.
35. Felson DT, Gale DR, Elon Gale M, Niu J, Hunter DJ, Goggins J, et al. Osteophytes and progression of knee osteoarthritis. *Rheumatology (Oxford)* 2005;44:100–4.
36. Garantzios S, Savani RC. Hyaluronan biology: a complex balancing act of structure, function, location and context. *Matrix Biol* 2019;78–79:1–10.
37. Bayliss MT, Howat S, Davidson C, Dudhia J. The organization of aggrecan in human articular cartilage: evidence for age-related changes in the rate of aggregation of newly synthesized molecules. *J Biol Chem* 2000;275:6321–7.
38. Lundell A, Olin AI, Morgelin M, al-Karadaghi S, Aspberg A, Logan DT. Structural basis for interactions between tenascins and lectican C-type lectin domains: evidence for a crosslinking role for tenascins. *Structure* 2004;12:1495–506.
39. Olin AI, Morgelin M, Sasaki T, Timpl R, Heinegard D, Aspberg A. The proteoglycans aggrecan and versican form networks with fibulin-2 through their lectin domain binding. *J Biol Chem* 2001;276:1253–61.
40. Dudhia J, Davidson CM, Wells TM, Hardingham TE, Bayliss MT. Studies on the G3 domain of aggrecan from human cartilage. *Ann N Y Acad Sci* 1996;785:245–7.
41. Clark IC. Articular cartilage: a review and scanning electron microscopy study. I. The interterritorial fibrillar architecture [review]. *J Bone Joint Surg Br* 1971;53B:732–50.
42. Douglas T, Heinemann S, Bierbaum S, Scharnweber D, Worch H. Fibrillogenesis of collagen types I, II, and III with small leucine-rich proteoglycans decorin and biglycan. *Biomacromolecules* 2006;7:2388–93.
43. Bomer N, Cornelis FM, Ramos YF, den Hollander W, Storms L, van der Breggen R, et al. The effect of forced exercise on knee joints in *Dio2^{-/-}* mice: type II iodothyronine deiodinase-deficient mice are less prone to develop OA-like cartilage damage upon excessive mechanical stress. *Ann Rheum Dis* 2016;75:571–7.
44. Lv M, Zhou Y, Polson SW, Wan LQ, Wang M, Han L, et al. Identification of chondrocyte genes and signaling pathways in response to acute joint inflammation. *Sci Rep* 2019;9:93.
45. Bock HC, Michaeli P, Bode C, Schultz W, Kresse H, Herken R, et al. The small proteoglycans decorin and biglycan in human articular cartilage of late-stage osteoarthritis. *Osteoarthritis Cartilage* 2001;9:654–63.
46. Young AA, Smith MM, Smith SM, Cake MA, Ghosh P, Read RA, et al. Regional assessment of articular cartilage gene expression and small proteoglycan metabolism in an animal model of osteoarthritis. *Arthritis Res Ther* 2005;7:R852–61.
47. Melrose J, Fuller ES, Roughley PJ, Smith MM, Kerr B, Hughes CE, et al. Fragmentation of decorin, biglycan, lumican and keratan is elevated in degenerate human meniscus, knee and hip articular cartilages compared with age-matched macroscopically normal and control tissues. *Arthritis Res Ther* 2008;10:R79.
48. Carames B, Olmer M, Kiosses WB, Lotz MK. The relationship of autophagy defects to cartilage damage during joint aging in a mouse model. *Arthritis Rheumatol* 2015;67:1568–76.
49. Gubbiotti MA, Neill T, Frey H, Schaefer L, Iozzo RV. Decorin is an autophagy-inducible proteoglycan and is required for proper in vivo autophagy. *Matrix Biol* 2015;48:14–25.

Supporting Information

Mediation of Cartilage Matrix Degeneration and Fibrillation by Decorin in Post-traumatic Osteoarthritis

*Qing Li,¹ Biao Han,¹ Chao Wang,¹ Wei Tong,² Yulong Wei,²
Wei-Ju Tseng,² Li-Hsin Han,³ X. Sherry Liu,² Motomi Enomoto-Iwamoto,⁴
Robert L. Mauck,^{2,5} Ling Qin,² Renato V. Iozzo,⁶ David E. Birk,⁷ Lin Han^{1,*}*

¹School of Biomedical Engineering, Science and Health Systems, Drexel University,
Philadelphia, PA 19104, United States

²McKay Orthopaedic Research Laboratory, Department of Orthopaedic Surgery, Perelman School of
Medicine, University of Pennsylvania, Philadelphia, PA 19104, United States

³Department of Mechanical Engineering and Mechanics, Drexel University,
Philadelphia, PA 19104, United States

⁴Department of Orthopaedics, School of Medicine, University of Maryland,
Baltimore, MD 21201, United States

⁵Translational Musculoskeletal Research Center, Corporal Michael J. Crescenz Veterans Administration
Medical Center, Philadelphia, PA 19104, United States

⁶Department of Pathology, Anatomy, and Cell Biology, Sidney Kimmel Medical College,
Thomas Jefferson University, Philadelphia, PA 19107, United States

⁷Department of Molecular Pharmacology and Physiology, Morsani School of Medicine,
University of South Florida, Tampa, FL 33612, United States

*Correspondence and requests for materials should be addressed to:

Dr. Lin Han

Phone: (215)571-3821

Fax: (215)895-4983

Email: lh535@drexel.edu.

Table S1. List of primers used for quantitative PCR

Gene	Forward Primer	Reverse Primer
<i>Dcn</i>	5'-TGAGCTTCAACAGCATCACC-3'	5'-AAGTCATTTTGCCCAACTGC-3'
<i>Acan</i>	5'-GACTGTGTGGTGATGATCTG-3'	5'-CTCGTAGCGATCTTCTTCTG-3'
<i>Col2a1</i>	5'-GCTGGTGCACAAGGTCCTAT-3'	5'-ACCTGCAGTCCAGTGAAAC-3'
<i>Bgn</i>	5'-CTACGCCCTGGTCTTGGTAA-3'	5'-ACTTTGCGGATACGGTTGTC-3'
<i>Adamts4</i>	5'-AGGTAAGGCCTCAGTCAGCA-3'	5'-AAGGAGCACAGACGATGCTT-3'
<i>Adamts5</i>	5'-TTGCTCTCCTCGAAGTGGTT-3'	5'-ATGGGTCTGGAGATCGAGTG-3'
<i>Mmp3</i>	5'-GATCTCTTCATTTTGGCCATCTCTTC-3'	5'-CTCCAGTATTTGTCTCTACAAAGAA-3'
<i>Mmp9</i>	5'-GGAACCTCACACGACATCTTCCA-3'	5'-GAAACTCACACGCCAGAAGAATTT-3'
<i>Mmp13</i>	5'-CCTTCTGGTCTTCTGGCACAC-3'	5'-GGCTGGGTACACTTCTCTG-3'
<i>Actb</i>	5'-AGATGACCCAGATCATGTTTGAGA-3'	5'-CACAGCCTGGATGGCTACGT-3'
<i>Gapdh</i>	5'-TCAACAGCAACTCCCACTCTTCCA-3'	5'-ACCCTGTTGCTGTAGCCGTATTCA-3'

Table S2. Summary of structural and biomechanical analysis outcomes of wild-type (WT) and decorin-null (*Dcn*^{-/-}) joints at 2 and 8 weeks post-surgery, shown as mean ± 95% CI from values averaged by each animal, except for κ as mean [95%CI]

2 weeks	Sham			DMM			<i>p</i> -value (Sham vs DMM)		<i>n</i>		Unit
	WT	<i>Dcn</i> ^{-/-}	<i>p</i>	WT	<i>Dcn</i> ^{-/-}	<i>p</i>	WT	<i>Dcn</i> ^{-/-}	WT	<i>Dcn</i> ^{-/-}	
<i>l</i> _{uncalcified, femur}	40 ± 7	43 ± 6	0.589	41 ± 7	41 ± 6	0.818	0.844	0.688	6	6	μm
<i>l</i> _{total, femur}	110 ± 17	110 ± 15	0.937	107 ± 15	108 ± 15	0.818	0.844	1.000	6	6	
<i>l</i> _{uncalcified, tibia}	53 ± 4	57 ± 5	0.093	53 ± 4	51 ± 5	0.589	1.000	0.026	6	6	
<i>l</i> _{total, tibia}	124 ± 8	126 ± 9	0.818	128 ± 13	122 ± 12	0.240	0.394	0.485	6	6	
Mankin Score	0.33 ± 0.54	2.33 ± 0.86	0.006	0.67 ± 0.54	4.17 ± 0.54	0.002	0.317	0.034	6	6	a.u.
<i>E</i> _{ind}	1.54 ± 0.20	0.47 ± 0.12	0.004	0.58 ± 0.19	0.41 ± 0.20	0.177	0.031	0.625	6	5	MPa
κ	0.37 [0.23 0.53]	0.40 [0.26 0.56]	0.963	0.38 [0.24 0.54]	1.39 [1.10 1.67]	< 0.001	0.869	< 0.001	4	4	--
8 weeks	Sham			DMM			<i>p</i> -value (Sham vs DMM)		<i>N</i>		Unit
	WT	<i>Dcn</i> ^{-/-}	<i>p</i>	WT	<i>Dcn</i> ^{-/-}	<i>p</i>	WT	<i>Dcn</i> ^{-/-}	WT	<i>Dcn</i> ^{-/-}	
<i>l</i> _{uncalcified, femur}	42 ± 7	40 ± 6	0.132	27 ± 2	20 ± 3	0.002	0.031	0.031	6	6	μm
<i>l</i> _{total, femur}	116 ± 10	107 ± 16	0.240	100 ± 16	82 ± 5	0.002	0.031	0.031	6	6	
<i>l</i> _{uncalcified, tibia}	55 ± 5	53 ± 5	0.310	34 ± 3	27 ± 7	0.041	0.002	0.002	6	6	
<i>l</i> _{total, tibia}	125 ± 11	120 ± 7	0.485	113 ± 13	91 ± 9	0.180	0.002	0.002	6	6	
Mankin Score	1.22 ± 0.42	2.72 ± 0.92	0.006	5.86 ± 1.02	8.10 ± 0.55	0.002	0.031	0.031	6	6	a.u.
<i>E</i> _{ind}	1.67 ± 0.46	0.44 ± 0.21	< 0.001	0.29 ± 0.08	0.18 ± 0.08	0.029	0.008	0.031	8	6	MPa
κ	0.35 [0.22 0.50]	0.42 [0.27 0.58]	0.690	0.40 [0.25 0.56]	3.30 [2.73 3.93]	< 0.001	0.793	< 0.001	4	4	--
SBP.Th	124 ± 41	108 ± 18	0.690	124 ± 23	128 ± 13	0.841	0.813	0.125	5	5	μm
STB BV/TV	50 ± 18	40 ± 11	0.190	54 ± 16	48 ± 8	0.421	0.138	0.043	5	5	%
STB Tb.N	6.8 ± 1.4	6.2 ± 0.9	0.310	6.8 ± 1.3	6.5 ± 0.9	0.421	0.225	0.043	5	5	mm ⁻¹
STB Tb.Th	89 ± 24	67 ± 19	0.095	103 ± 28	90 ± 8	0.222	0.138	0.043	5	5	μm
Men. OV _{ant.}	96 ± 6	85 ± 5	0.016	204 ± 67	158 ± 48	0.310	0.043	0.043	5	5	× 10 ⁻³
Men. OV _{post.}	13 ± 10	22 ± 10	0.151	42 ± 24	80 ± 30	0.056	0.043	0.043	5	5	mm ³

Table S3. Summary of structural and biomechanical analysis outcomes of control and decorin inducible knockout (*Dcn^{iKO}*) joints at 8 weeks post-surgery, shown as mean \pm 95% CI from the values averaged by each animal, except for κ as mean [95%CI]

8 weeks	Sham			DMM			<i>p</i> -value (Sham vs DMM)		<i>n</i>		Unit
	Control	<i>Dcn^{iKO}</i>	<i>p</i>	Control	<i>Dcn^{iKO}</i>	<i>p</i>	Control	<i>Dcn^{iKO}</i>	Ctrl	<i>Dcn^{iKO}</i>	
<i>t</i> _{uncalcified, femur}	37 \pm 5	42 \pm 5	0.180	43 \pm 7	40 \pm 9	0.589	0.180	1.000	6	6	μm
<i>t</i> _{total, femur}	120 \pm 10	124 \pm 9	0.589	99 \pm 11	93 \pm 11	0.310	0.004	0.002	6	6	
<i>t</i> _{uncalcified, tibia}	56 \pm 9	57 \pm 4	0.485	53 \pm 7	48 \pm 9	0.310	0.699	0.065	6	6	
<i>t</i> _{total, tibia}	125 \pm 12	130 \pm 8	0.589	112 \pm 13	106 \pm 10	0.394	0.093	0.002	6	6	
Mankin Score	0.72 \pm 0.60	1.00 \pm 0.80	0.732	5.72 \pm 0.46	7.17 \pm 0.28	0.002	0.031	0.031	6	6	a.u.
<i>E</i> _{ind}	1.24 \pm 0.34	1.18 \pm 0.24	0.690	0.41 \pm 0.23	0.64 \pm 0.21	0.095	0.043	0.043	5	5	MPa
κ	0.36 [0.27 0.46]	0.24 [0.17 0.32]	0.245	0.32 [0.23 0.41]	2.17 [1.96 2.38]	< 0.001	0.690	< 0.001	4	4	--
SBP.Th	136 \pm 28	134 \pm 10	1.000	130 \pm 22	150 \pm 17	0.222	0.438	0.125	5	5	μm
STB BV/TV	56 \pm 10	53 \pm 12	1.000	57 \pm 6	64 \pm 10	0.151	0.500	0.043	5	5	%
STB Tb.N	7.0 \pm 0.8	7.6 \pm 1.1	0.310	7.7 \pm 0.5	8.7 \pm 1.0	0.056	0.043	0.043	5	5	mm ⁻¹
STB Tb.Th	89 \pm 21	82 \pm 9	0.690	95 \pm 17	102 \pm 6	0.841	0.138	0.043	5	5	μm
Men. OV _{ant.}	93 \pm 2	86 \pm 16	0.548	216 \pm 75	165 \pm 39	0.151	0.043	0.043	5	5	$\times 10^{-3}$
Men. OV _{post.}	30 \pm 17	39 \pm 18	0.548	54 \pm 37	103 \pm 59	0.056	0.043	0.043	5	5	mm ³

Table S4. Summary of qPCR and DMMB analysis outcomes from *in vitro* live explant culture, shown as mean \pm 95% from values averaged by each biological repeat

Live Explant	Untreated			IL-1 β			<i>p</i> -value (Untr. vs IL-1 β)		<i>n</i>		Unit
	WT	<i>Dcn^{-/-}</i>	<i>p</i>	WT	<i>Dcn^{-/-}</i>	<i>p</i>	WT	<i>Dcn^{-/-}</i>	WT	<i>Dcn^{-/-}</i>	
<i>Dcn</i>	1.00 \pm 0.43	0.06 \pm 0.04	0.002	1.98 \pm 0.53	0.06 \pm 0.03	0.002	0.004	0.485	6	6	relative mRNA (to WT without IL-1 β)
<i>Acan</i>	1.00 \pm 0.15	1.04 \pm 0.30	0.937	0.57 \pm 0.16	0.80 \pm 0.38	0.394	0.002	0.310	6	6	
<i>Col2a1</i>	1.00 \pm 0.43	0.98 \pm 0.56	0.818	0.54 \pm 0.26	0.71 \pm 0.21	0.310	0.026	0.589	6	6	
<i>Bgn</i>	1.00 \pm 0.24	0.83 \pm 0.38	0.310	1.05 \pm 0.36	0.92 \pm 0.25	0.310	0.937	0.699	6	6	
<i>Adamts4</i>	1.00 \pm 0.79	1.14 \pm 0.34	0.394	13.9 \pm 10.1	16.3 \pm 7.9	0.394	0.002	0.002	6	6	
<i>Adamts5</i>	1.00 \pm 0.48	1.18 \pm 0.59	0.699	75.8 \pm 23.3	73.6 \pm 20.4	0.818	0.002	0.002	6	6	
<i>Mmp3</i>	1.00 \pm 0.48	1.00 \pm 0.56	0.965	109 \pm 43	98 \pm 30	1.000	0.002	0.002	6	6	
<i>Mmp9</i>	1.00 \pm 0.41	1.06 \pm 0.45	0.818	7.06 \pm 2.09	6.64 \pm 3.15	0.699	0.002	0.002	6	6	
<i>Mmp13</i>	1.00 \pm 0.49	0.90 \pm 0.41	0.699	34.3 \pm 10.9	36.8 \pm 10.3	0.589	0.002	0.002	6	6	
sGAG media	12.6 \pm 2.8	10.5 \pm 2.8	0.180	23.2 \pm 5.8	18.4 \pm 4.2	0.093	0.002	0.002	6	6	$\mu\text{g}/\text{mg}$ wet wt.
sGAG expl.	58.7 \pm 6.8	28.2 \pm 7.8	0.002	48.8 \pm 10.9	18.6 \pm 3.0	0.002	0.093	0.015	6	6	
sGAG total	71.3 \pm 4.9	38.8 \pm 6.4	0.002	72.0 \pm 8.2	37.1 \pm 3.1	0.002	0.937	0.818	6	6	
Loss ratio	17.9 \pm 4.5	28.0 \pm 9.4	0.132	32.6 \pm 9.4	49.5 \pm 8.6	0.015	0.004	0.002	6	6	%

Table S5. Summary of DMMB analysis outcomes from *in vitro* devitalized explant culture, shown as mean \pm 95% from values averaged by each biological repeat

ADAMTS-5	Untreated			Treated			<i>p</i> -value (untr. vs treated)		<i>n</i>		Unit
	WT	<i>Dcn</i> ^{-/-}	<i>p</i>	WT	<i>Dcn</i> ^{-/-}	<i>p</i>	WT	<i>Dcn</i> ^{-/-}	WT	<i>Dcn</i> ^{-/-}	
sGAG media	9.7 \pm 2.1	10.5 \pm 3.3	0.937	25.6 \pm 5.3	27.4 \pm 5.3	0.699	0.002	0.002	6	6	μ g/mg wet wt.
sGAG expl.	61.8 \pm 7.0	32.0 \pm 8.3	0.002	45.7 \pm 9.5	18.4 \pm 7.8	0.002	0.015	0.015	6	6	
sGAG total	71.5 \pm 8.2	42.6 \pm 6.6	0.002	71.3 \pm 8.0	45.8 \pm 4.8	0.002	0.818	0.394	6	6	
Loss ratio	13.5 \pm 2.3	25.5 \pm 9.7	0.009	36.2 \pm 7.8	60.3 \pm 13.1	0.026	0.002	0.002	6	6	%
MMP-13	Untreated			Treated			<i>p</i> -value (untr. vs treated)		<i>n</i>		Unit
	WT	<i>Dcn</i> ^{-/-}	<i>p</i>	WT	<i>Dcn</i> ^{-/-}	<i>p</i>	WT	<i>Dcn</i> ^{-/-}	WT	<i>Dcn</i> ^{-/-}	
sGAG media	13.4 \pm 1.9	14.3 \pm 2.2	0.485	18.4 \pm 1.6	25.2 \pm 2.2	0.002	0.002	0.002	6	6	μ g/mg wet wt.
sGAG expl.	61.1 \pm 3.7	31.6 \pm 3.4	0.002	54.8 \pm 3.2	19.1 \pm 4.0	0.002	0.009	0.002	6	6	
sGAG total	74.5 \pm 3.6	46.0 \pm 3.8	0.002	73.2 \pm 4.3	44.3 \pm 2.6	0.002	0.485	0.589	6	6	
Loss ratio	18.0 \pm 2.6	31.2 \pm 4.3	0.002	25.1 \pm 1.4	57.2 \pm 6.6	0.002	0.002	0.002	6	6	%

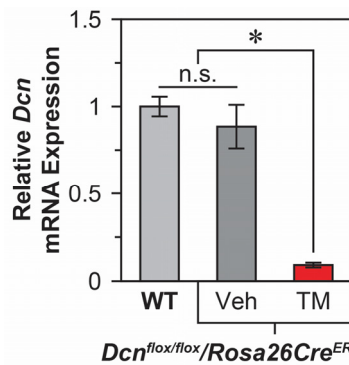


Figure S1. Confirmation of the induced knockout of *Dcn* gene in *Dcn*^{iKO} mice via tamoxifen administration. In 3-month-old *Dcn*^{fllox/fllox}/*Rosa26Cre*^{ER} mice, intraperitoneal (i.p.) injection of 3 mg tamoxifen (TM)/40 g body weight for 3 consecutive days reduces the expression of decorin (*Dcn*) to the baseline level (mean \pm SEM, *n* = 5 animals, *: *p* < 0.01 via Mann-Whitney U test), as tested on day 5, while injection of vehicle (Veh) does not alter the level of *Dcn* expression relative to the wild-type (WT) (*p* = 0.421).

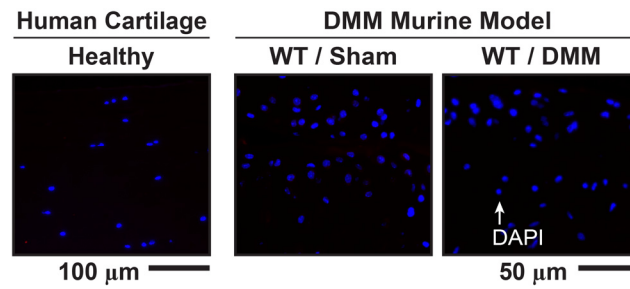


Figure S2. Isotype control images of decorin immunofluorescence (IF) on healthy human articular cartilage and WT murine knee cartilage at 8 weeks after Sham and DMM surgeries (blue: DAPI).

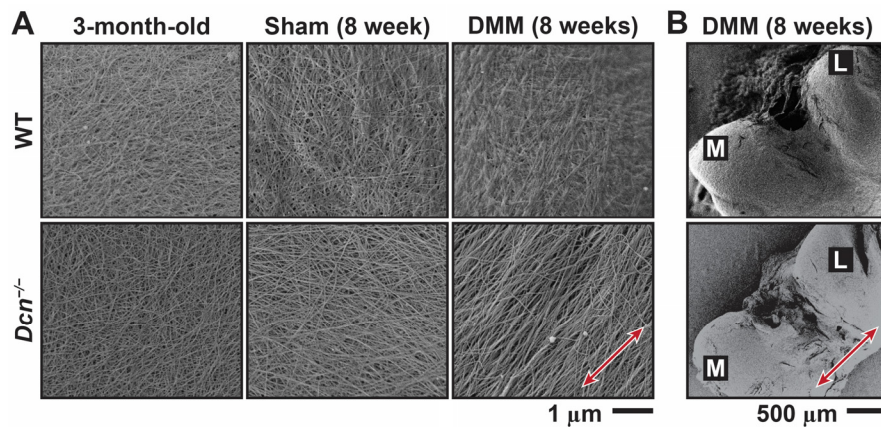


Figure S3. Scanning electron microscope (SEM) images of murine knee cartilage surfaces. A) Representative images of WT and *Dcn*^{-/-} cartilage surfaces from 3-month-old, un-operated mice and from mice at 8 weeks after DMM or Sham surgeries. B) Corresponding low-resolution images of knee joints show that the surface fibrils become aligned along the mediolateral direction on *Dcn*^{-/-} cartilage surface after DMM (L: lateral side, M: medial side).

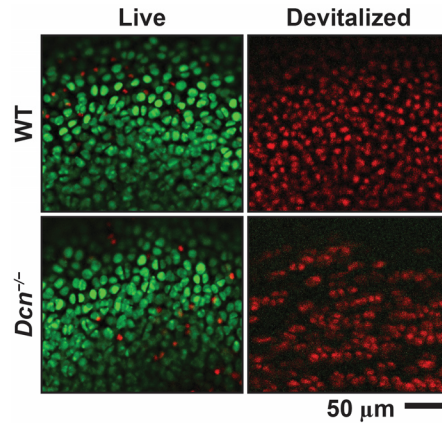


Figure S4. Confirmation of cell viability in live and devitalized cartilage explants via cell live/dead assay. Immediately after harvesting, the live explants were sterilized and pre-cultured in standard chondrogenic DMEM at 37°C for 2 days, and the devitalized explants underwent three freeze-thaw cycles between –80°C for 2 h and at 37°C for 45 min. Both explants were then stained and imaged via the fluorescein diacetate (FDA) and propidium iodide (PI) staining method.

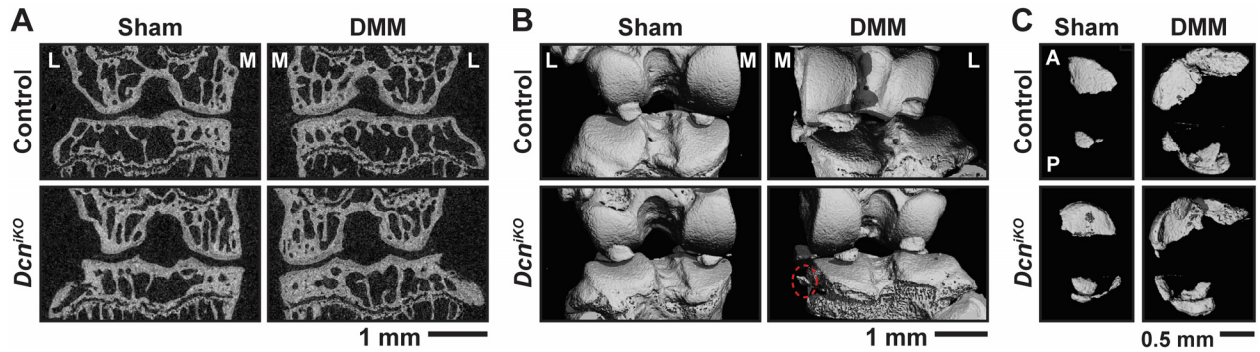


Figure S5. Representative μ CT images of *Dcn^{iKO}* and control mice at 8 weeks after surgery. A) Representative 2D μ CT frontal plane images of the knee joint (L: lateral, M: medial). B) Representative reconstructed 3D μ CT images show the presence of osteophyte in *Dcn^{iKO}* mice after DMM (red ellipse), but not in other groups. C) Representative reconstructed 3D μ CT images (top view) of medial meniscal ossicles show increased ossification after DMM in both genotypes (A: anterior, P: posterior).